Chapter 5

The Application of Periodic Density Functional Theory to the Study of Uranyl-Containing Materials: Thermodynamic Properties and Stability

Francisco Colmenero Ruiz

Additional information is available at the end of the chapter

http://dx.doi.org/10.5772/intechopen.79558

Abstract

With the advent of increased computer capacities, improved computational resources, and easier access to large-scale computer facilities, the use of density functional theory methods has become nowadays a frequently used and highly successful approach for the research of solid-state materials. However, the study of solid materials containing heavy elements as lanthanide and actinide elements is very complex due to the large size of these atoms and the requirement of including relativistic effects. These features impose the availability of large computational resources and the use of high quality relativistic pseudopotentials for the description of the electrons localized in the inner shells of these atoms. The important case of the description of uranyl-containing materials and their properties has been faced recently. The study of these materials is very important in the energetic and environmental disciplines. Uranyl-containing materials are fundamental components of the paragenetic sequence of secondary phases that results from the weathering of uraninite ore deposits and are also prominent phases appearing from the alteration of the spent nuclear fuel. The development of a new norm-conserving relativistic pseudopotential for uranium, the use of energy density functionals specific for solids, and the inclusion of empirical dispersion corrections for describing the long-range interactions present in the structures of these materials have allowed the study of the properties of these materials with an unprecedented accuracy level. This feature is very relevant because these methods provide a safe, accurate, and cheap manner of obtaining these properties for uranium-containing materials which are highly radiotoxic, and their experimental studies demand a careful handling of the samples used. In this work, the results of recent applications of theoretical solid state methods based on density functional theory using plane waves and pseudopotentials to the determination of the thermodynamic properties and stability of uranyl-containing materials are reviewed. The knowledge of these thermodynamic properties is indispensable to model the dynamical behavior of nuclear materials under diverse geochemical conditions. The theoretical methods provide

a profound understanding of the thermodynamic stability of these mineral phases and represent a powerful predictive tool to determine their thermodynamic properties.

Keywords: uranyl-containing minerals, spent nuclear fuel, density functional theory, thermodynamic stability, heat capacities, entropies, enthalpies, Gibbs free energies, thermodynamic properties of formation, Gibbs free energies of reaction

1. Introduction

The basis of thermodynamic theory [1] is known since the end of the nineteenth century, and the fundamental developments carried out in the twentieth century have established this theory as a self-contained system of knowledge. The thermodynamic calculations are mainly used for the description of the changes of state associated with the transfer of matter and energy and are an indispensable part of technical and scientific investigations in various fields such as chemistry, metallurgy, chemical engineering, and the energy and environmental technologies. The reliability of the results of thermochemical calculations depends, in the first instance, on the accuracy of the thermochemical data used and the inclusion of the most important species involved, which are often quite numerous if one desires to obtain a fair description of real systems.

There are different sources of data available for establishing thermodynamic information such as calorimetric and solubility measurements [2, 3], phase equilibrium data [4], experimental data on solid solutions [5], and heat capacities and entropies estimated from lattice vibrational models [6–8]. Reasonably complete sets of basic data needed for the calculation of thermochemical functions are available only for a relatively small number of substances [9], and frequently these sets must be completed with empirical data of lower accuracy obtained by analyzing values from different sources as well as by performing estimations before they can be used for actual calculations.

The data listed in the thermochemical tables generally form databases [10–18, 4]. An internally consistent database is one which permits the computation of phase equilibrium relations as established by experimental studies, and it is at the same time compatible with calorimetric and other measurements of thermochemical properties of the phases involved. The generation of such databases is very complex due to the large uncertainties associated with phase equilibrium studies at high temperature and pressure and because many experiments may be irreversible. The CALPHAD method (CALculation of PHAse Diagrams) [19, 20] may be used in the derivation and assessment of this kind of databases [21].

These databases can be used to carry out thermodynamic multi-component, multi-phase, multi-reaction equilibrium calculations on systems made up of any of the substances present in the database. These calculations are best performed by adopting the method of minimization of the total Gibbs free energy of the closed system [22–28]. A detailed description of the principles and techniques used in the computation of equilibrium assemblages of a closed system can be found in the work of Smith and Missen [24]. Thus, these databases are the basis

http://dx.doi.org/10.5772/intechopen.79558

for the software packages for the calculation of equilibria in multi-component systems [12, 13, 18, 19, 22, 23, 29–32]. Examples of successful applications of thermodynamic techniques to the computation of equilibrium phase assemblages in geological and planetary systems have been reported [33–36].

In the field of nuclear technology, the thermodynamic information is indispensable in order to predict the chemical behavior and dynamics of nuclear materials under diverse environmental conditions. The knowledge of precise thermodynamic data is fundamental for the development of geochemical models for nuclear fuel degradation, to evaluate the origin and evolution of uranium ore bodies, in developing programs for the solution mining of uranium deposits or mine dumps, in the study of spent nuclear fuel (SNF) radioactive waste and in the containment of such waste, and may also be of importance in reactions within breeder reactors [37–41].

The behavior of a deep geologic repository (DGR) of high level radioactive waste (HLWR) will depend mainly on the interaction between the SNF and their surroundings. The hydration and corrosion of the SNF under oxidizing conditions will result in the dissolution of the uranium dioxide composing the SNF matrix and the formation of uranyl secondary mineral phases [42–54]. Therefore, the formation and stability of uranyl minerals will determine the release of U(VI) and other actinide elements from the HLWR container and subsequently from the repository to the biosphere [55–70].

The stabilities and dissolution rates of uranyl minerals are functions of the solution composition, temperature, and local conditions (mainly pH and electrochemical potential), and their prediction requires the knowledge of the Gibbs free energy, enthalpy, and entropy thermodynamic functions of formation for each phase of interest and their variation with temperature. The simulation of the release of uranium from DGRs under oxidizing conditions and the mobility of uranium in the environment can be only performed if the thermodynamic properties of the secondary uranyl minerals that may form in the DGR are available. Consequently, the knowledge of the thermodynamic parameters is crucial for predicting DGR performance [71–73]. However, reliable temperature-dependent thermodynamic data are completely lacking, except for the simplest uranyl-containing materials. Therefore, the development of a complete thermodynamic database for these minerals is mandatory.

The rapid development of the nuclear technology strongly encouraged the research on the field of thermodynamics of nuclear materials and the development of nuclear thermodynamic databases [74, 75]. The great significance of the thermodynamic information of materials containing uranium and related elements in the assessment of the safety of DGRs is reflected by the large number of recent experimental works leading to large reviews and updates of thermodynamic properties of materials [72–77]. Among these studies, we may remark the recent experimental measurements by means of solubility and calorimetry techniques of the thermodynamic properties of uranyl peroxide hydrates [51–54], uranyl carbonate minerals [78], uranyl phosphate and orthophosphate minerals [79], and uranyl silicates [71, 80–84].

Despite of the fast progress in the generation of the nuclear thermodynamic database, there are many uranium-containing materials for which the corresponding data are unreliable due to the large experimental uncertainties [38]. A large amount of effort has been dedicated to the

assignment and correction of these uncertainties by means of the implementation of new statistical methods for hypothesis testing and the improvement of the techniques used for measuring the thermodynamic properties of these systems [73]. The need to make available a comprehensive, internationally recognized and quality assured chemical thermodynamic database that meets the modeling requirements for the safety assessment of radioactive waste disposal systems prompted the Radioactive Waste Management Committee (RWMC) of the Organization for Economic Co-operation and Development (OECD) Nuclear Energy Agency (NEA) to launch the Thermochemical Database Project (NEA TDB). The RWMC assigned a high priority to the critical review of relevant chemical thermodynamic data of inorganic species, actinide compounds, and fission products [72, 73]. Besides, the range of conditions of temperature and pressure for which the thermodynamic parameters are available for most nuclear materials is rather limited.

While the knowledge of the temperature dependence of these properties for anhydrous uranium oxides is very complete [73–75], the corresponding data for the secondary phases which arise from alteration of SNF under final DGR conditions are surprisingly scarce. For these secondary phases, the thermodynamic parameters are known only for the standard state (298.15 K and 1 bar). The lack of temperature-dependent information for these phases rules out the possibility of performing reliable thermodynamic modeling studies for the performance assessment of DGRs for SNF. Because the corresponding information is available for anhydrous species, thermodynamic computations have been performed for the uranium-oxygen and sodium-uranium-oxygen system [85–95]. A detailed analysis of previous studies [41, 96–105] suggests that first principles methodology is an excellent complement to experimental methodology for determining the thermodynamic functions of these materials.

In this work, the computation of the thermodynamic properties of a large set of uranyl-containing materials is reviewed [99–105]. This set includes the uranyl peroxide studtite [$(UO_2)O_2{\cdot}4H_2O$] and metastudtite [$(UO_2)O_2{\cdot}2H_2O$], the uranyl hydroxide dehydrated schoepite [$UO_2(OH)_2$], the uranyl oxyhydroxide schoepite [$(UO_2)_8O_2(OH)_{12}{\cdot}12H_2O$], metaschoepite [$(UO_2)_8O_2(OH)_{12}{\cdot}10H_2O$] and becquerelite [$Ca(UO_2)_6O_4(OH)_6{\cdot}8H_2O$], the uranyl silicate soddyite [$(UO_2)_2(SiO_4){\cdot}2H_2O$], the uranyl carbonate rutherfordine [UO_2CO_3], and gamma uranium trioxide [γ-UO_3]. The first eight materials have been identified to be basic components of the paragenetic sequence of secondary phases arising from the alteration of uraninite ore deposits and corrosion of SNF under the final DGR conditions [42–54], and gamma uranium trioxide is the main oxide of hexavalent uranium [100, 106, 107]. Uranyl peroxides appear in the earlier stages of this paragenetic sequence [50–54, 108–111] due to the production of hydrogen peroxide and other oxidants resulting from the radiolysis of water due to the ionizing radiation of the SNF. The uranyl oxyhydroxides also begin to appear soon from the alteration of uranium dioxide [42–48]. Studtite, schoepite, metaschoepite, and becquerelite phases have been observed as alteration products of spent fuel in cooling basins at the Hanford Site (Washington) [112–116] and on Chernobyl "lava" formed during the nuclear accident that occurred in 1986 [117]. The next mineral phases appearing in this sequence are uranyl silicates and, less frequently, uranyl phosphates [42–48]. Uranyl carbonates may precipitate where the evaporation is significant, and the carbon dioxide partial pressure is large [49, 118]. The main ingredients of this paragenetic sequence were inferred by Frondel already in 1956 [42, 43]. The sequence is still widely accepted

http://dx.doi.org/10.5772/intechopen.79558

today [44–48, 118, 119]. However, our knowledge of this sequence is only qualitative, and the performance assessment of the DGRs for HLRW and many other applications in nuclear technology require its quantitative specification.

The crystal structures of these materials [100, 102, 105, 120–123] were successfully determined by means of density functional theory using plane waves and pseudopotentials [124]. A new norm-conserving relativistic pseudopotential specific for uranium atom was generated from first principles with this purpose [101, 121]. Then, using these optimized structures, the thermodynamic properties of these materials were determined including specific heats, entropies, enthalpies, and Gibbs free energies [99–105]. The computed thermodynamic properties were combined with those of the corresponding elements in order to determine the enthalpy and free energy of formation of these materials and its variation with temperature [102, 104, 105]. The methods used in the computation of these thermodynamic functions are briefly described in Section 2. Additionally, the calculation of the Gibbs free energies of reaction and associated reaction constants is also described in this section. The main results obtained are described in Section 3, including a study of the thermodynamic stability of the secondary phases of SNF [102, 104, 105]. Finally, the main conclusions are given in Section 4.

2. Methods

2.1. Computational methodology

The generalized gradient approximation (GGA) together with PBE functional [125] supplemented with Grimme empirical dispersion correction [126] was used to study the uranyl-containing materials such as studtite, metastudtite, dehydrated schoepite, schoepite, metaschoepite, becquerelite, soddyite, rutherfordine, and gamma uranium trioxide [99–105, 120–123]. The introduction of dispersion corrections improved significantly the computed structural, vibrational, mechanic and thermodynamic properties of studtite, metastudtite, dehydrated schoepite, schoepite, metaschoepite, becquerelite, and soddyite as a consequence of the better description of the hydrogen bonding present in the crystal structures of these materials. However, for the case of rutherfordine and gamma uranium trioxide phases, the specialized version of PBE functional for solid materials, PBEsol [127], provided much better results [99, 100, 121]. The improved description of the structure of properties of anhydrous materials using this functional over the one obtained using PBE was observed in recent calculations [99, 100, 121] and later confirmed by other research groups [128, 129]. This justifies the great amount of effort made in developing density functionals specific for solid materials [130] and emphasizes the need of determining empirical dispersion parameters specific for these functionals. These functionals are implemented in CASTEP program [131], a module of the Materials Studio package [132], which was employed to model the structures of the materials considered. The pseudopotentials used for H, C, O, Si, and Ca atoms in the unit cells of these minerals were standard norm-conserving pseudopotentials [133] given in CASTEP code (00PBE-OP type). The norm-conserving relativistic pseudopotential for U atom was generated from first principles as shown in the previous works [101, 121]. While our uranium atom pseudopotential includes scalar relativistic effects, the corresponding

pseudopotentials used for H, C, O, Si, and Ca atoms do not include them. This pseudopotential has been used extensively in the research of uranyl-containing materials [99–105, 120–123].

The atomic positions and cell parameters were optimized using the Broyden-Fletcher--Goldfarb-Shanno method [124, 134] with a convergence threshold on atomic forces of 0.01 eV/Å. The kinetic energy cut-off and K-point mesh [135] were chosen to ensure good convergence for computed structures and energies. The structures of the materials considered in this work were optimized in calculations with augmented complexity by increasing these parameters. The precise calculation parameters used to determine the final results may be found in the corresponding articles [99–105, 120–123]. The flow diagram associated to the theoretical treatment used to study a given crystalline material is shown in **Figure 1** [101]. The crystal structure is first optimized starting from an initial atomistic model of the corresponding unit cell (lattice parameters and atomic positions) employing trial values of the calculation parameters (kinetic energy cut-off and K-point mesh). The crystal structure is then updated and the initial values of the kinetic cutoff and K-point density (number of k-points divided by the k-point separation) are systematically increased. The geometry optimization is performed again until the variation of the energy is below a given threshold. The variation of the crystal unit cell is then analyzed, and the structure is reoptimized until this variation is small enough. Once the convergence in the computed energy and structure is met, the

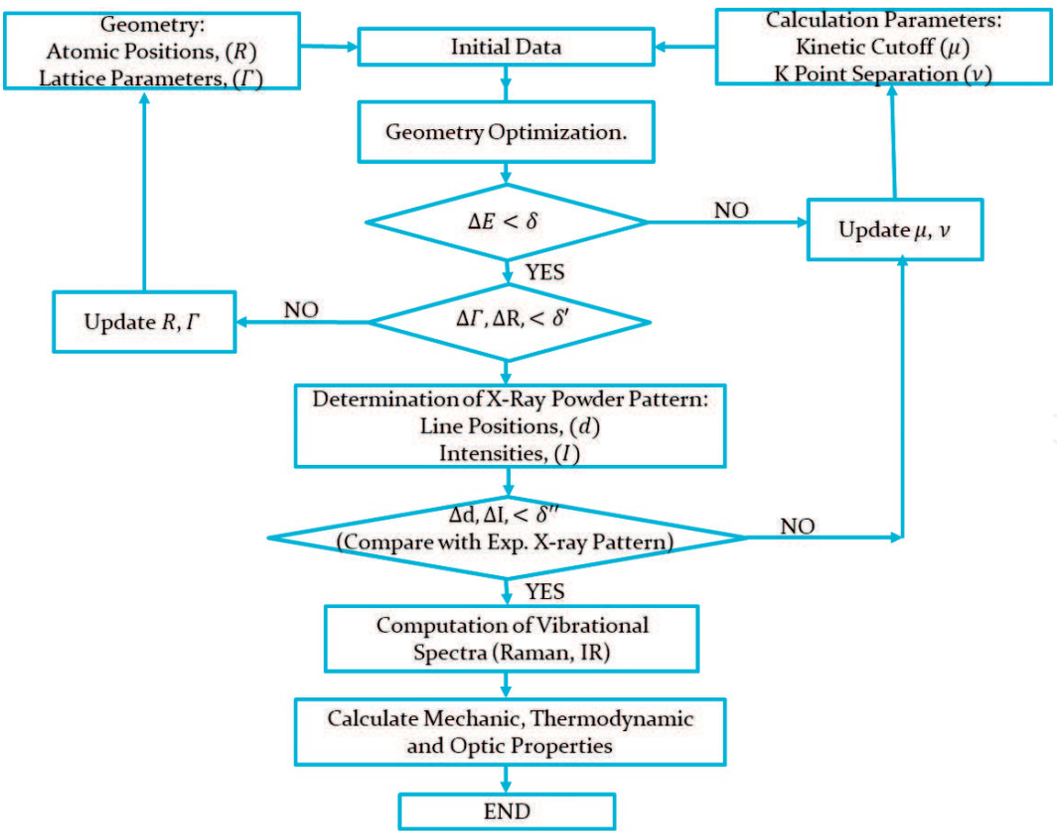

Figure 1. Flow diagram associated to the theoretical solid state treatment used to study the uranyl-containing materials considered in this work.

corresponding X-ray powder pattern is determined [136] and compared with the experimental one. Only if the comparison is satisfactory, the crystal structure is accepted in order to obtain the final vibrational, mechanic, thermodynamic, and optic properties of the material under study. Otherwise, the calculation parameters are made more stringent and the structural optimization starts again. The convergence of this procedure depends on the proximity of the initial input used to the final solution. If it does not converge or converges towards a structure yielding an X-ray powder pattern which does not agree with the experimental one, the procedure should be restarted from a different initial input (atomic positions and cell parameters).

2.2. Thermodynamic properties

The methods employed for the calculation of thermodynamic properties of these materials were described in the previous papers [99–105]. The phonon spectrum at the different points of Brillouin zone can be determined by density functional perturbation theory (DFPT) [137–139] as second-order derivatives of the total energy [137]. Phonon dispersion curves and density of states were calculated, and from them, several important thermodynamic quantities in the quasi-harmonic approximation, such as Gibbs free energy, enthalpy, entropy, and specific heat, were evaluated [140].

2.3. Enthalpy and Gibbs free energy of formation in terms of the elements

The thermodynamic functions of formation at the different temperatures were determined [102] from the calculated enthalpy and entropy functions of the material being considered, $[H_T\text{-}H_{298}]^{calc}$ and S_T^{calc}, the experimental value of its standard enthalpy of formation, $\Delta_f H^0$, and the experimental enthalpy and entropy functions of the elements forming part of the material. The enthalpy and entropy functions for the elements were taken from JANAF tables [11], and the corresponding functions for uranium atom were taken from Barin [12]. The equilibrium constants for the formation reactions were determined in terms of the corresponding calculated Gibbs free energies of formation using the well-known relationship [11], $\Delta_f G(T) = -\ R\ T\ Ln\ K_f$.

2.4. Enthalpies and free energies of reaction

The enthalpies and Gibbs free energies of a given reaction at the different temperatures, $\Delta_r H(T)$ and $\Delta_r G(T)$, were determined [103] from the Gibbs free energy of formation and entropy functions of the materials entering in the reaction, $\Delta_f G^i(T)$ and $S^i(T)$, $i = 1,\ldots,N_{mat}$. The specific values used of these properties for studtite, metastudtite, dehydrated schoepite, schoepite, metaschoepite, becquerelite, soddyite, rutherfordine, and gamma uranium trioxide were determined in our previous works [102, 104, 105]. The corresponding data for the remaining materials, which do not contain the uranyl ion, SiO_2(cr), H_2O(l), CO_2(g), O_2(g), and H_2(g), were taken from JANAF tables [11] and the data for H_2O_2(l) were taken from Barin [12]. The reaction equilibrium constants were determined in terms of the corresponding Gibbs free energies of reaction, $\Delta_r G(T) = -\ R\ T\ Ln\ K_r$.

3. Results and discussion

3.1. Thermodynamic properties

The computed isobaric heats and entropies at 298.15 K for all the uranyl-containing materials considered in this work [99, 100, 102, 104, 105] are given in **Table 1**. In this table, the values obtained for rutherfordine, gamma uranium trioxide, and metaschoepite [99, 100, 104] are compared with the corresponding experimental values. For the rest of the materials, there are not experimental values to compare with. As it can be seen, the computed values agree very well with their experimental counterparts. In fact, the differences between the computed and experimental values of these and other thermodynamic properties are frequently smaller than the difference among several different experimental values. From the analysis of the results obtained, the expected accuracy in the computed-specific heats and entropies of studtite, metastudtite, dehydrated schoepite, schoepite, and soddyite is better than 3–5%.

The calculated isobaric specific heat, entropy, and Gibbs free energy functions of rutherfordine, gamma uranium trioxide, and metaschoepite are displayed in **Figure 2**, where they are compared with the experimental functions of Hemingway [37], Cordfunke and Westrum [143], and Barin [12], respectively. For rutherfordine, the computed thermodynamic functions are compared with those of Hemingway [37] in the temperature range of 298–700 K, and as it can be appreciated, the calculated and experimental curves are nearly parallel. The computed value of C_p at 700 K, near the limit of thermal stability of rutherfordine [37], C_p = 153.3 J K^{-1} mol^{-1}, differs from the experimental value at this temperature, 147.6 J · K^{-1} mol^{-1}, by only 3.9%.

Material	Source	C_p	S
Rutherfordine	Calc. [99]	115.02	143.11
	Exp.	106.5 [37] (8.0%), 120.1 [141] (−5.1%)	142.70 [37] (0.3%), 139 [142] (3.0%)
γ-UO_3	Calc. [100]	77.36	92.96
	Exp.	81.67 [143] (−5.3%), 84.72 [37] (−8.7%)	96.11 [143] (−3.3%), 98.6 [144] (−5.7%)
Metaschoepite	Calc. [104]	142.01	166.24
	Exp.	154.40 [12] (−8.0%)	167.00 [12] (−0.5%)
Studtite	Calc. [102]	219.97, 211.17 [41]	232.12
Metastudtite	Calc. [102]	163.14, 155.81 [41]	179.27
Dehydrated schoepite	Calc. [102]	103.85	125.18
Schoepite	Calc. [104]	150.62	168.75
Soddyite	Calc. [102]	275.15	315.95
Becquerelite	Calc. [105]	148.40	172.34

All the values are given in units of J K^{-1} mol^{-1}. The percent difference of the theoretical and experimental results is given in parenthesis for the specific heats and entropies of rutherfordine, gamma uranium trioxide, and metaschoepite.

Table 1. Specific heats and entropies at 298.15 K for the uranyl-containing material studied in this work.

http://dx.doi.org/10.5772/intechopen.79558

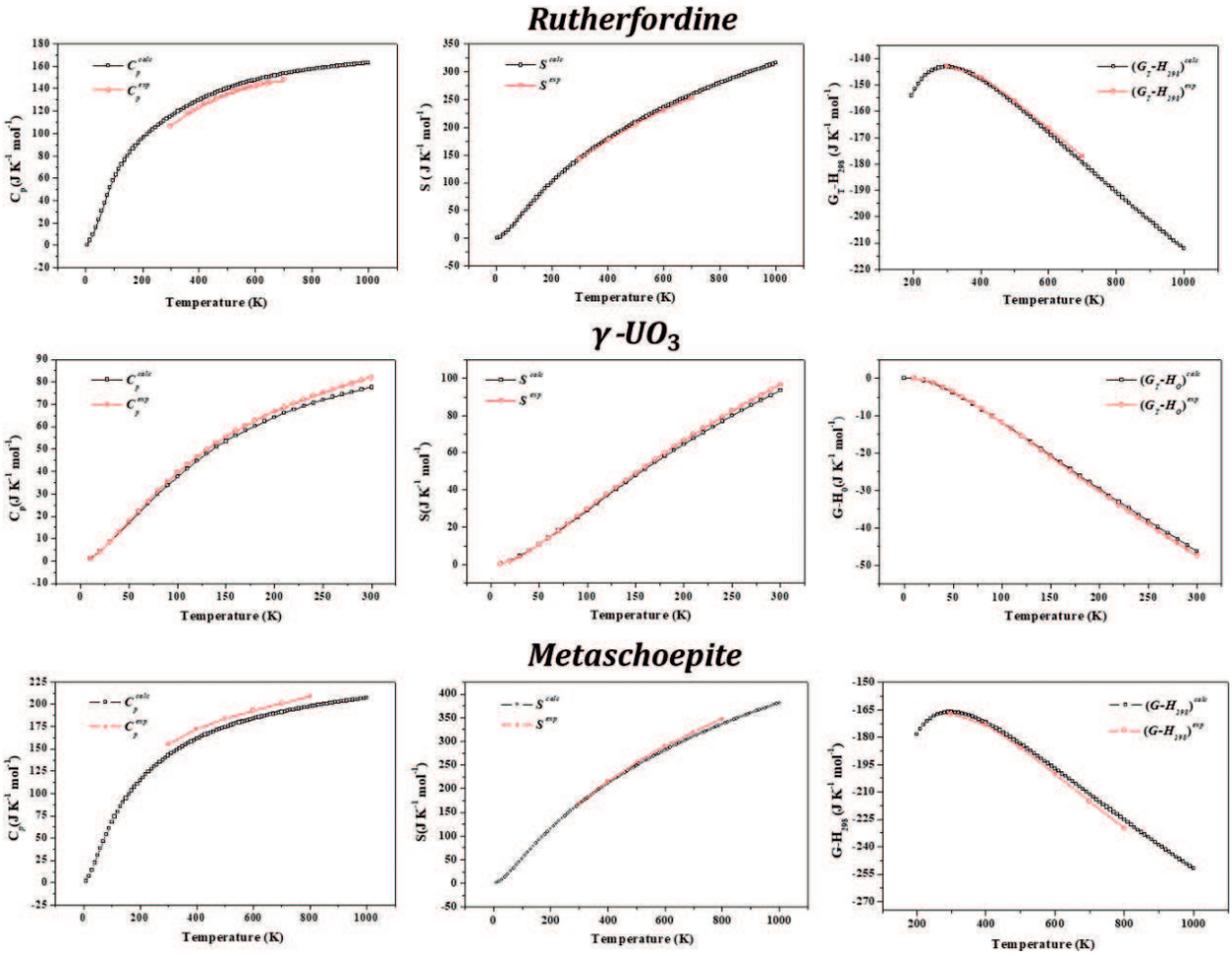

Figure 2. Calculated and experimental isobaric specific heat entropies and Gibbs free energies of rutherfordine, gamma uranium trioxide, and metaschoepite as a function of temperature. The experimental thermodynamic functions of rutherfordine, uranium trioxide, and metaschoepite are from Hemingway [37], Cordfunke and Westrum [143], and Barin [12], respectively.

Similarly, the differences of the computed entropy and Gibbs free energy with respect to Hemingway's experimental values at 700 K are only 2.3 and 1.3%, respectively. Our theoretical calculations allowed to obtain the values of the thermodynamic functions for the low and high temperature ranges 0–300 and 700–1000 K, which were unknown so far and, consequently, extended the range in which the thermodynamic functions were known to 0–1000 K.

The computed thermodynamic properties of uranium trioxide are also in excellent agreement with the experimental data of Cordfunke and Westrum [143] in the full range of temperatures considered 0–1000 K. The differences in the specific heat, entropy, and Gibbs free energy functions are 3.9, 1.8, and 0.1% at 100 K and 6.1, 3.6, and 3.5% at 1000 K. The comparison reveals that the low temperature calculated thermodynamic data are also very accurate. It must be emphasized that while the experimental isobaric heat capacity function of gamma uranium trioxide at 1000 K is above the asymptotic Dulong-Petit limit, our computed function satisfies properly the requirement of being below this limit [100].

Finally, the theoretical results for metaschoepite mineral phase agree very well with the experimental thermodynamic properties reported by Barin [12] even at temperatures of the order of 800 K, the percent differences of the calculated specific heat, entropy, and Gibbs energy with respect to the corresponding experimental values being 5.4%, 3.2%, and 2.0% at 800 K. The present theoretical data have permitted to discriminate between the experimental thermodynamic functions of metaschoepite reported up to date because the experimental functions reported by Tasker et al. [145] deviate from those of Barin [12] and from our theoretical results already at moderate temperatures [104].

The comparisons performed in the previous paragraph have shown that the variation of the computed thermodynamic functions with temperature is excellent. Hence, it may be expected that the theoretical functions obtained for studtite, metastudtite, dehydrated schoepite, soddyite, schoepite, and becquerelite [102, 104, 105] will also be reliable even at low and high temperatures. For rutherfordine and metaschoepite [99, 104], the calculated thermodynamic properties are recommended instead of the experimental functions because they cover the full temperature range going from 0 to 1000 K and they should provide a uniform accuracy at all temperatures. For gamma uranium trioxide, both sets of data are considered to be equally accurate, but the theoretical specific heat function satisfies properly the asymptotic conditions [100].

3.2. Enthalpies and free energies of formation in terms of the elements

The enthalpies and free energies of formation in terms of the elements of the considered mineral phases as a function or temperature were determined [102, 104, 105] from the calculated thermodynamic data, the experimental or estimated [104] standard enthalpy of formation, and the thermodynamic functions of the corresponding elements [11–12]. The calculated Gibbs free energies of formation of rutherfordine, gamma uranium trioxide, and metaschoepite [102, 104] are shown in **Figure 3** together with the corresponding experimental data [12, 37, 143].

As it may be observed in **Figure 3**, and as it occurred with the thermodynamic functions of the pure substances reported in Section 3.1, the calculated thermodynamic properties of formation agree with the experimental functions in an excellent manner. For these three materials, the differences of the calculated and experimental values are lower than 1% at ambient temperature and the differences remain very small at high temperatures. The differences become 1.6%, 1.0%, and 2.0% at 700, 900, and 800 K for rutherfordine, γ-UO_3, and metaschoepite, respectively [102, 104]. Since the theoretical solid state treatments used for studtite, metastudtite, dehydrated schoepite, soddyite, schoepite, and becquerelite were essentially the same as those used for these three materials, we expect a similar accuracy level for their calculated thermodynamic parameters of formation. An example of these calculated parameters for a material in which there are no experimental data to compare with is the case of the schoepite mineral phase, and the corresponding results are also shown in **Figure 3**. The combination of the results for schoepite and metaschoepite allowed to study the thermodynamics of the dehydration transformation of schoepite into metaschoepite [104].

http://dx.doi.org/10.5772/intechopen.79558

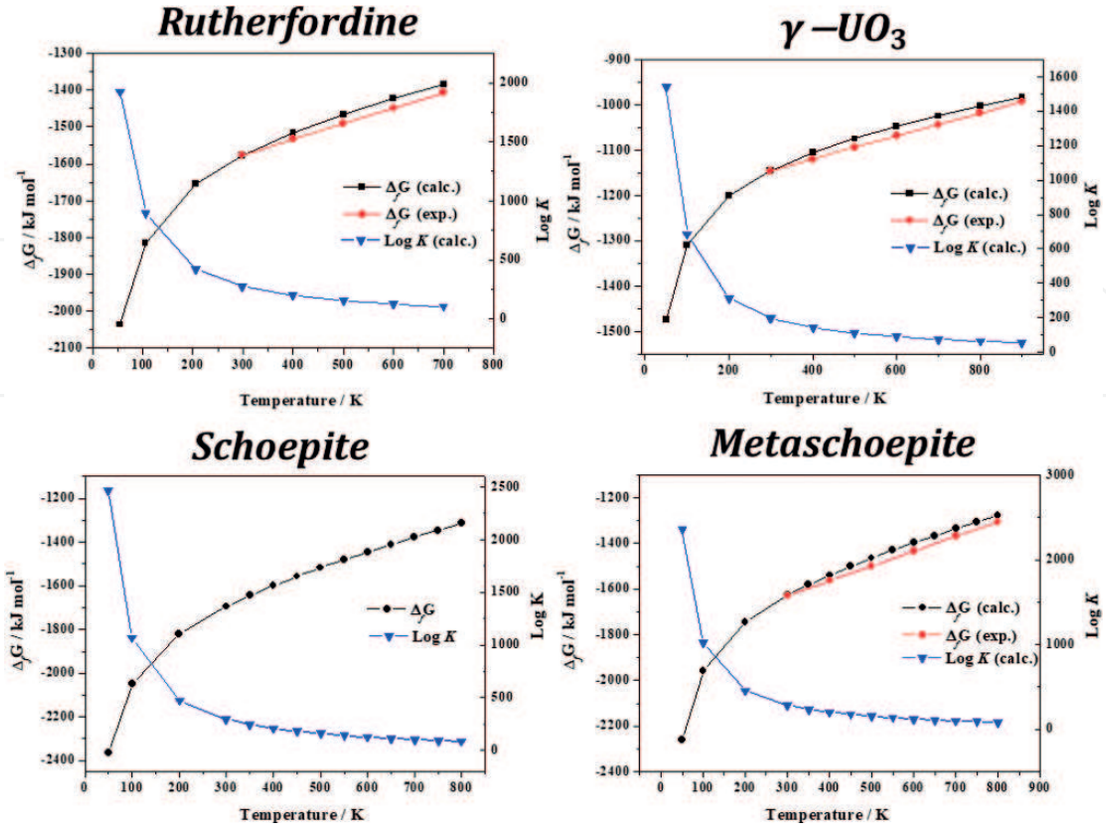

Figure 3. Calculated Gibbs free energies of formation of rutherfordine, gamma uranium trioxide, and metaschoepite in terms of the elements as a function of temperature. The experimental Gibbs free energies of formation of rutherfordine, uranium trioxide, and metaschoepite are from Hemingway [37], Cordfunke and Westrum [143], and Barin [12], respectively. For schoepite, there are no experimental data to compare with.

3.3. Enthalpies and free energies of reaction

3.3.1. Reactions of formation in terms of oxides

Let us first consider the following reactions:

$$\text{Studtite: } UO_3(cr) + 4\,H_2O(l) + 1/2O_2(g) \rightarrow (UO_2)O_2 \cdot 4H_2O(cr) \quad \text{(I)}$$

$$\text{Metastudtite: } UO_3(cr) + 2\,H_2O(l) + 1/2O_2(g) \rightarrow (UO_2)O_2 \cdot 2H_2O(cr) \quad \text{(II)}$$

$$\text{Dehydrated schoepite: } UO_3(cr) + H_2O(l) \rightarrow UO_2(OH)_2(cr) \quad \text{(III)}$$

$$\text{Becquerelite: } UO_3(cr) + 1/6\,CaO(cr) + 11/6H_2O(l) \rightarrow 1/6\,Ca(UO_2)_6O_4(OH)_6 \cdot 8H_2O(cr) \quad \text{(IV)}$$

$$\text{Schoepite: } UO_3(cr) + 9/4\,H_2O(l) \rightarrow 1/8\left[(UO_2)_8O_2(OH)_{12}\right] \cdot 12H_2O(cr) \quad \text{(V)}$$

$$\text{Metaschoepite: } UO_3(cr) + 2\,H_2O(l) \rightarrow 1/8\left[(UO_2)_8O_2(OH)_{12}\right] \cdot 10\,H_2O(cr) \quad \text{(VI)}$$

$$\text{Rutherfordine: } UO_3(cr) + CO_2(g) \rightarrow UO_2CO_3(cr) \quad \text{(VII)}$$

$$\text{Soddyite : } 2UO_3(cr) + SiO_2(cr) + 2H_2O(l) \rightarrow (UO_2)_2(SiO_4) \cdot 2H_2O(cr) \quad \text{(VIII)}$$

These important reactions represent the formation of the considered uranyl-containing materials in terms of the corresponding oxides. By combining the calculated thermodynamic properties of formation of these materials in terms of the elements [102, 104, 105] with those of the non-uranyl-bearing materials [11] present in reactions (I)–(VIII), we obtained the Gibbs free energies and associated reaction constants displayed in **Figure 4** [103–105].

Figure 4 shows that studtite and metastudtite are unstable with respect to the corresponding oxides at the full range of temperatures studied, 250–500 K, since the corresponding Gibbs free energies of reaction are positive everywhere. Therefore, they are metastable phases at normal conditions. The opposite is true for soddyite mineral phase, which is stable at all the temperatures. However, dehydrated schoepite, becquerelite, schoepite, metaschoepite, and rutherfordine mineral phases are stable at ambient temperature and become unstable at the temperatures of 462, 491, 383, 352, and 514 K, respectively, because the Gibbs free energy of reaction becomes positive at these temperatures. The observation of changes of stability for these phases at these relatively low temperatures was unexpected and highlights the great relevance of the availability of accurate temperature-dependent thermodynamic functions [102, 103].

3.3.2. Reactions of transformation of uranyl-containing materials into studtite in the presence of high hydrogen peroxide concentrations

We will now study the thermodynamic properties of the following set of reactions:

$$UO_2(OH)_2(cr) + 2\,H_2O_2(l) + H_2(g) \rightarrow (UO_2)O_2 \cdot 4H_2O(cr) \quad \text{(IX)}$$

$$1/2\,(UO_2)_2(SiO_4) \cdot 2H_2O(cr) + 2\,H_2O_2(l) + H_2(g) \rightarrow (UO_2)O_2 \cdot 4H_2O(cr) + 1/2\,SiO_2(cr) \quad \text{(X)}$$

$$UO_3(cr) + 3\,H_2O_2(l) + H_2(g) \rightarrow (UO_2)O_2 \cdot 4H_2O(cr) + 1/2\,O_2(g) \quad \text{(XI)}$$

$$UO_2CO_3(cr) + 3\,H_2O_2(l) + H_2(g) \rightarrow (UO_2)O_2 \cdot 4H_2O(cr) + CO_2(g) + 1/2O_2(g) \quad \text{(XII)}$$

$$(UO_2)O_2 \cdot 2H_2O(cr) + H_2O_2(l) + H_2(g) \rightarrow (UO_2)O_2 \cdot 4H_2O(cr) \quad \text{(XIII)}$$

$$1/6\,Ca(UO_2)_6O_4(OH)_6 \cdot 8H_2O(cr) + 13/6\,H_2O_2(l) \rightarrow (UO_2)O_2 \cdot 4H_2O(cr) + 1/16\,CaO(cr) + 7/12\,O_2(g) \quad \text{(XIV)}$$

$$1/8\left[(UO_2)_8O_2(OH)_{12}\right] \cdot 12H_2O(cr) + 7/4\,H_2O_2(l) \rightarrow (UO_2)O_2 \cdot 4H_2O(cr) + 3/8\,O_2(g) \quad \text{(XV)}$$

$$1/8\left[(UO_2)_8O_2(OH)_{12}\right] \cdot 12H_2O(cr) + 1/8\,O_2(g) \rightarrow 1/8\left[(UO_2)_8O_2(OH)_{12}\right] \cdot 10\,H_2O(cr) + 1/4\,H_2O_2(l) \quad \text{(XVI)}$$

Reactions (IX) to (XV) are the reactions of transformation of dehydrated schoepite, soddyite, uranium trioxide, rutherfordine, metastudtite, becquerelite, and schoepite into studtite in the presence of high hydrogen peroxide concentrations (and absence of water) [103–105]. Reaction (XVI) represents the conversion of schoepite into metaschoepite at these conditions. The computed Gibbs free energies of these reactions are shown in **Figure 5**. As it can be observed, all

http://dx.doi.org/10.5772/intechopen.79558

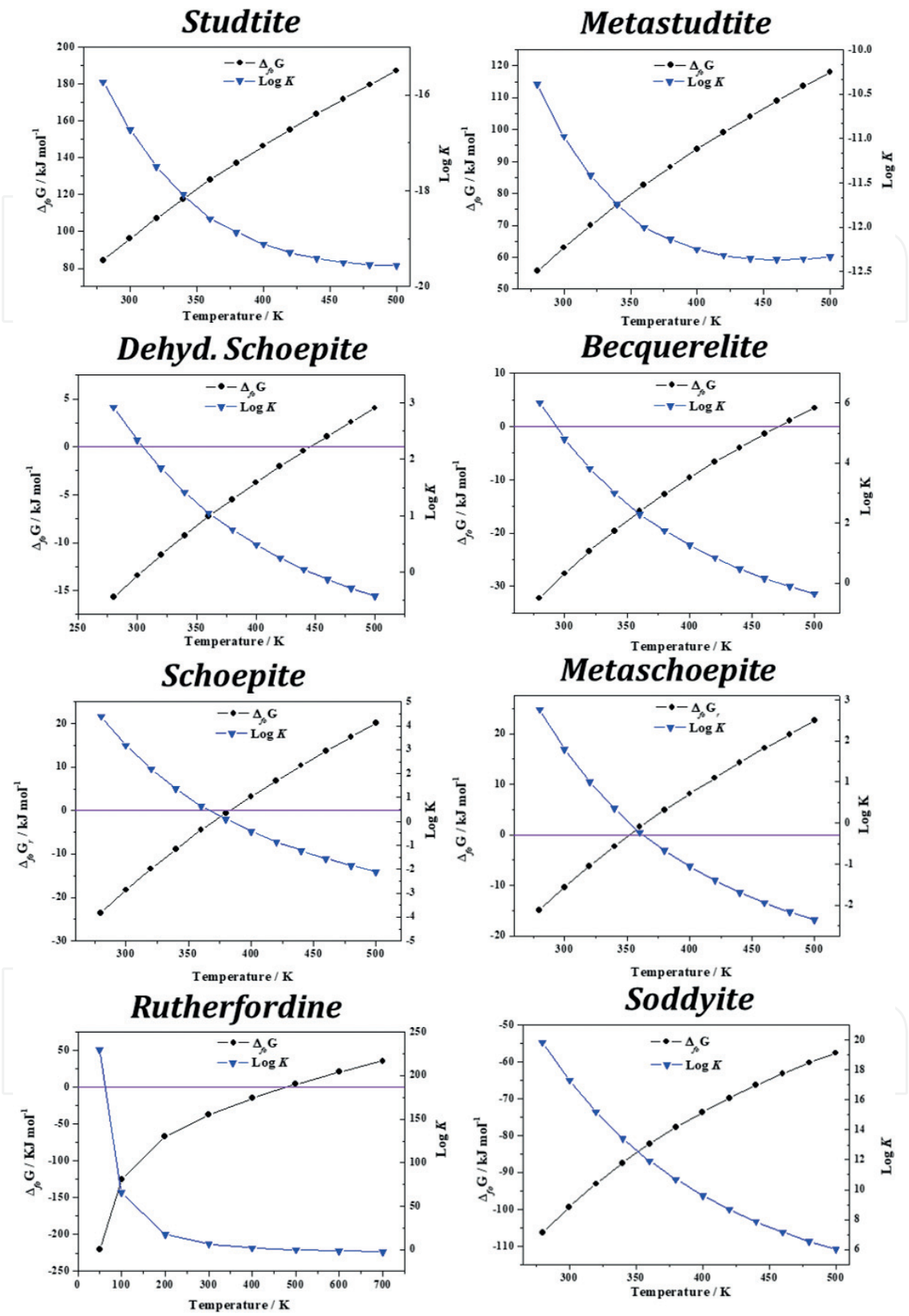

Figure 4. Calculated Gibbs free energies of formation of studtite, metastudtite, dehydrated schoepite, becquerelite, schoepite, metaschoepite, rutherfordine, and soddyite in terms of the corresponding oxides as a function of temperature [103–105].

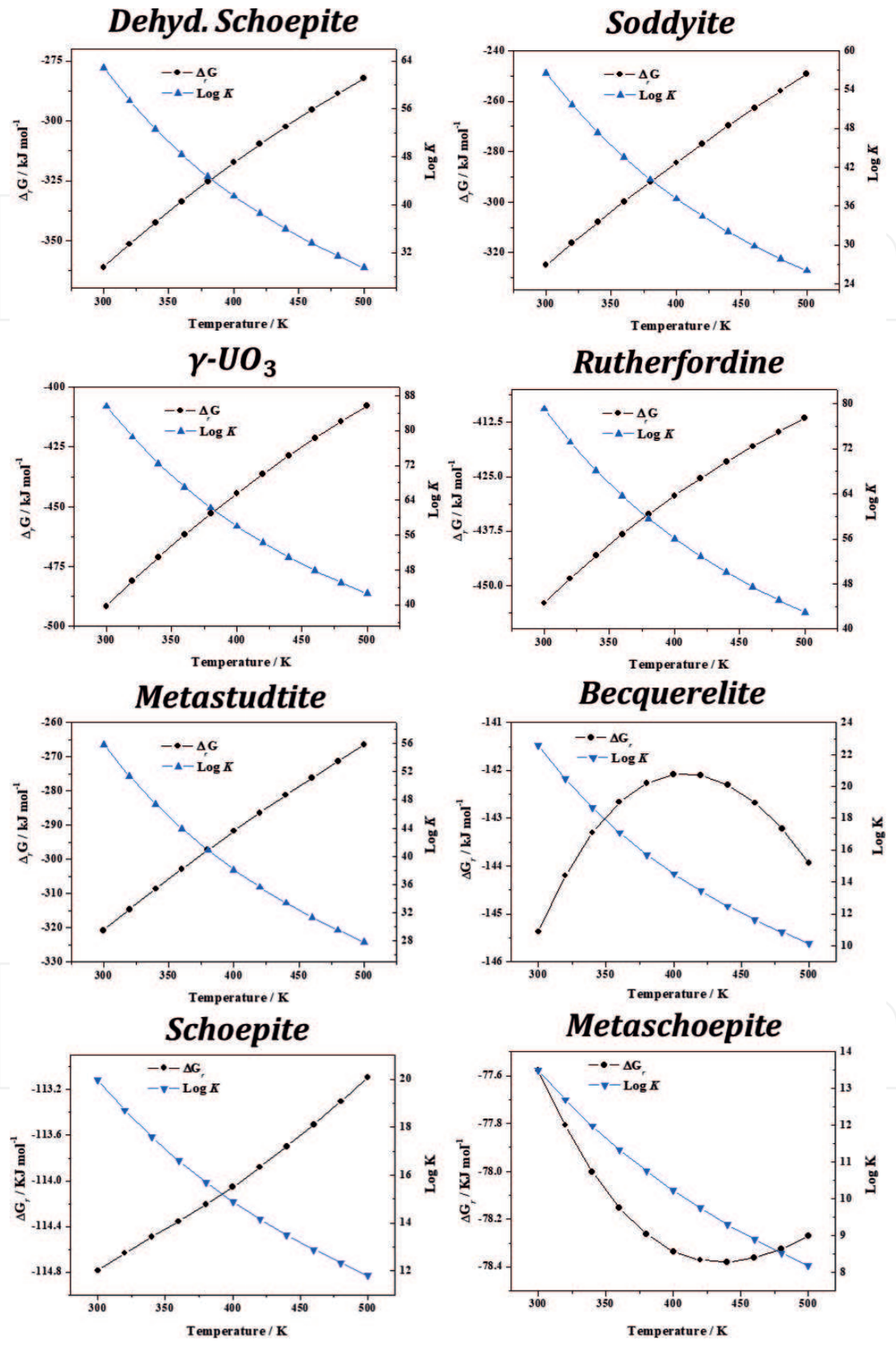

Figure 5. Calculated Gibbs free energies of the reactions of transformation of dehydrated schoepite, soddyite, gamma uranium trioxide, rutherfordine, metastudtite, becquerelite, and schoepite into studtite and of metaschoepite into schoepite in the presence of high hydrogen peroxide concentrations as a function of temperature [103–105].

these phases will transform spontaneously into studtite in the presence of high hydrogen peroxide concentrations, since the Gibbs free energy of all these reactions are negative for the full range of temperatures considered, 300–500 K. In the case of metaschoepite, the thermodynamics of reaction (XVI) shows that it will convert into schoepite mineral phase, but according to reaction (XV) the last phase also transforms spontaneously into studtite [104].

Forbes et al. [110] investigated experimentally the transformation of dehydrated schoepite and soddyite into studtite phase in solutions with large concentrations of hydrogen peroxide. They observed that, at ambient temperature, these materials transform into studtite following the reaction stoichiometry. The results of our calculations [103] for the conversion of dehydrated schoepite and soddyite under high hydrogen peroxide concentrations into studtite agree completely with this experimental study. However, our results extend this study because it shows that the same will happen not only at 298.15 K but also at temperature as high as 500 K. The study performed by Kubatko et al. [146] showed that becquerelite mineral phase also transforms into studtite within 8 hours under high hydrogen peroxide concentrations. The thermodynamics of the conversion of becquerelite into studtite under variable concentrations of hydrogen peroxide was studied by our group in a recent paper [105]. The results displayed in **Figure 4** [103–105] show that the same will happen for gamma uranium trioxide, rutherfordine, metastudtite, schoepite, and metaschoepite phases. In fact, because the stability of studtite under these conditions is very high, it is likely that the same will happen for most of the other secondary phases of SNF, as it was suggested in 2017 [101].

Our study of the thermodynamics of these reactions also permits to comprehend why uranyl peroxide hydrates were the unique phases found in a 2-year corrosion experiment of SNF in deionized water [109]. These phases should be the unique phases found not only in deionized water but also in water containing silicate ions, since studtite is much more stable than soddyite and probably more stable than most other uranyl silicate phases under high hydrogen peroxide concentrations.

3.4. Thermodynamic stability

From the thermodynamic data reported in our previous papers [103–105], the order of thermodynamic stability of the uranyl-containing materials considered in this work was evaluated as a function of temperature under three different conditions: (A) under high concentrations of hydrogen peroxide; (B) in the presence of water and hydrogen peroxide; and (C) in the absence of hydrogen peroxide. The stability of these phases at these conditions in the range of temperatures from 300 to 500 K is displayed in **Figures 5A** and **6B** and **C**. In these three figures, the relative stabilities are given with respect to studtite, metastudtite, and gamma uranium trioxide, respectively.

Figure 6 provides a very clear idea of the temporal evolution of the paragenetic sequence of secondary phases appearing as a result of the corrosion of SNF under final DGR conditions. Uranyl peroxide phase studtite will appear as the prominent phase at the earlier stages of this paragenetic sequence (see **Figure 6A**) due to the presence of high hydrogen peroxide concentrations caused by the radiolysis of most of the water reaching the surface of SNF. If the hydrogen peroxide concentration diminishes with time, as expected from the decrease of the

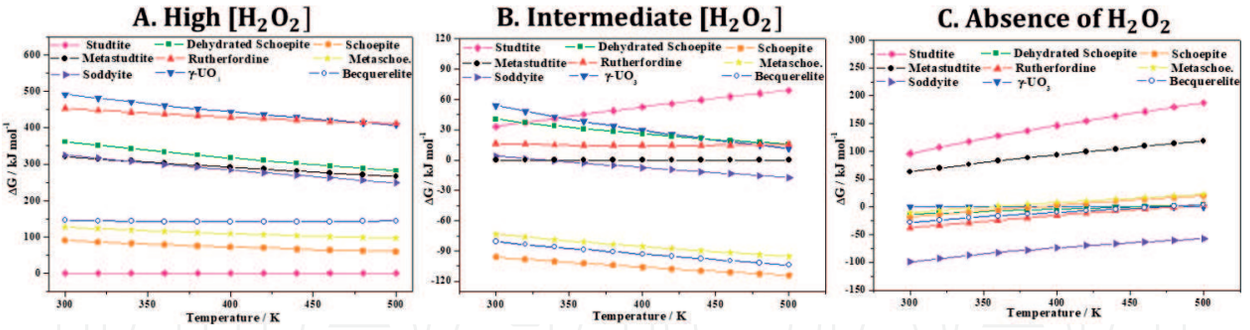

Figure 6. Relative thermodynamic stability of a selected set of secondary phases of SNF: (A) under high hydrogen peroxide concentrations; (B) under the presence of water and hydrogen peroxide; and (C) under the absence of hydrogen peroxide.

intensity of radiation fields over time in a DGR [147], the studtite stability will decrease and the formation of other secondary phases will occur. In the presence of water and hydrogen peroxide (see **Figure 6B**), the uranyl oxyhydroxide phases (schoepite, metaschoepite, and becquerelite) appear to be the most stable ones. Finally, in the absence of hydrogen peroxide, soddyite is the most stable phase and rutherfordine is also more stable than becquerelite for temperatures lower than 492 K (**Figure 6C**). Thus, at hydrogen peroxide free conditions, uranyl silicates and carbonates must be the most prominent phases of the SNF.

A full evaluation and understanding of the number and relative amount of the secondary phases of spent nuclear fuel present at the conditions of a final geological disposal over time require the realization of complete thermodynamic calculations employing thermochemical data for a significant number of materials, including the most important secondary phases, amorphous phases, and aqueous species, at a wide range of temperature and pressure conditions [103]. The determination of these thermodynamic data, the evaluation of their temperature and pressure dependence, and the realization of the corresponding thermodynamic computations are one of the main objectives of our current research.

3.5. Solubility constants

The important solubility reactions of schoepite, metaschoepite, rutherfordine, and becquerelite may be written, respectively, as follows:

$$1/8\left[(UO_2)_8O_2(OH)_{12}\right]\cdot 12H_2O(cr) + 2\,H^+(aq) \rightarrow UO_2{}^{2+}(aq) + 13/4\,H_2O(l) \quad \text{(XVII)}$$

$$1/8\left[(UO_2)_8O_2(OH)_{12}\right]\cdot 10H_2O(cr) + 2\,H^+(aq) \rightarrow UO_2{}^{2+}(aq) + 3\,H_2O(l) \quad \text{(XVIII)}$$

$$Ca(UO_2)_6O_4(OH)_6\cdot 8H_2O(cr) + 14\,H + (aq) \rightarrow Ca^{2+}(aq) + 6\,UO_2{}^{2+}(aq) + 16\,H_2O(l) \quad \text{(XIX)}$$

$$UO_2CO_3(cr) \rightarrow UO_2{}^{2+}(aq) + CO_3{}^{2-}(aq) \quad \text{(XX)}$$

Using the computed values of the Gibbs free energies of formation of schoepite, metaschoepite, becquerelite, and rutherfordine and the Gibbs free energies of formation of aqueous ions, $UO_2{}^{2+}$(aq),

http://dx.doi.org/10.5772/intechopen.79558

Material	$\Delta_{sp}G$ (calc.)	Log K_{sp} (calc.)	Log K_{sp} (exp.)
Schoepite	−26.11	4.57	—
Metaschoepite	−34.14	5.98	5.6 ± 0.2 [149], 5.52 ± 0.04 [150], 6.23 ± 0.14 [151], 5.9 ± 0.1 [152], 5.14 ± 0.05 [153], 5.72 ± 0.19 [154], 5.79 ± 0.19 [155]
Becquerelite	−287.55	50.38	40.5 ± 1.4 [149], 41.2 ± 0.52 [156], 43.2 [157], 29 ± 1 [158], 41.89 ± 0.52 [159], 43.70 ± 0.47 [159]
Rutherfordine	96.83	−16.96	−14.91 ± 0.10 [153], −13.89 ± 0.11 [154], −13.29 ± 0.01 [155]

The values of $\Delta_{sp}G$ Δ_rG are in units of $kJ{\cdot}mol^{-1}$.

Table 2. Calculated and experimental Gibbs free energies ($\Delta_{sp}G$) and associated reaction constants (Log K_{sp}) of the solubility reactions of schoepite, metaschoepite, becquerelite, and rutherfordine.

$UO_2^{2+}(aq)$, $CO_3^{2-}(aq)$, $Ca^{2+}(aq)$, and $H^+(aq)$, and liquid water at 298.15 K [148], one obtains the Gibbs free energies and associated reaction constants of solubility given in **Table 2**.

The calculated solubility products, $LogK_{sp}^{calc}$ of metaschoepite, becquerelite, and rutherfordine 5.98, 50.38, and −16.96 respectively, are in very good agreement with the most recent experimental values ($LogK_{sp}^{exp}$ = 5.6 ± 0.2 [149], 40.5 ± 1.4 [149], −14.91 ± 0.10 [153]). Since there solubility constant of schoepite has not been determined experimentally, its value was predicted [104]. Schoepite is shown to be more insoluble than metaschoepite.

4. Conclusions

It has been demonstrated [99–105, 120–123] that Periodic Density Functional Theory methods are an extremely powerful tool in the research of uranium-containing compounds. The use of the new relativistic norm-conserving pseudopotential [101, 121] permitted the computation of the structural properties, X-ray powder patterns, vibrational Raman spectra, and mechanical and thermodynamic properties of these materials. These methods are free of the problems involved in the experimental methods associated to the radiotoxicity of these compounds.

The first principles methodology allowed the safe, accurate, and cheap study of secondary phases of SNF definitive geological disposal conditions. The theoretical methods may be used, in conjunction with experimental techniques, as an interpretative tool of the experimental data or as a predictive tool to determine the structural, vibrational, mechanic, and thermodynamic properties of these substances. One of the most successful applications of this methodology has been achieved when studying their fundamental thermodynamic properties [99–105].

The development of empirical dispersion corrections [126] and the development of density functionals specific for solid materials [130] have improved extraordinarily the reliability of the calculated thermodynamic functions and their temperature dependence. The results were

shown to be accurate at very low and high temperatures [99–105]. The description of the temperature dependence of these functions is very difficult from the experimental point of view. The theoretical approach has permitted in some cases, as those of the rutherfordine [99] and metaschoepite [104] mineral phases, to extend the range of temperatures in which the thermodynamic properties were known and to determine the variation with temperature of these properties for a large series of important phases in which it was completely unknown: studtite, metastudtite, dehydrated schoepite, becquerelite, schoepite, and soddyite. Furthermore, the calculated thermodynamic functions satisfy properly the Dulong-Petit asymptotic constraints.

The comparison of the computed heat capacities and entropies with experimental data was very satisfactory in those cases in which there ware experimental data to compare with. The calculated Gibbs free energies of formation of rutherfordine, γ-UO_3, and metaschoepite [102, 104] were in good agreement with experiment at ambient temperature, and the differences with the corresponding experimental values were only 1.6%, 1.0%, and 2.0% at 700, 900, and 800 K, respectively. Because the theoretical treatments used for studtite, metastudtite, dehydrated schoepite, soddyite, schoepite, and becquerelite were essentially the same as those used for these three materials, we expect a similar accuracy level for their calculated thermodynamic parameters of formation [102, 104, 105].

As an application of the calculated thermodynamic properties of the considered uranyl materials, the Gibbs free energies and associated reaction constants of a large number of reactions involving these materials were determined. The results provided a deep and clear understanding of the temporal evolution of the paragenetic sequence of secondary phases appearing at the surface of SNF as a result of its corrosion under final DGR conditions [103–105]. Additional work is now in progress to determine the thermodynamic properties of a significant number of additional phases. The use of these thermodynamic parameters in detailed multi-component thermodynamic computations should be pursued in a near future.

Acknowledgements

Supercomputer time by the CETA-CIEMAT, CTI-CSIC, and CESGA centers is acknowledged. This work has been carried out in the context of a CSIC–CIEMAT collaboration agreement: "Caracterización experimental y teórica de fases secundarias y óxidos de uranio formados en condiciones de almacenamiento de combustible nuclear." I want to thank Dr. Ana María Fernández, Dr. Vicente Timon, Dr. Laura J. Bonales, Dr. Joaquín Cobos, and Dr. Rafael Escribano for their continuous help and advice during the realization of these studies.

Conflict of interest

The author declares that there is no conflict of interest.

Dedication

To Beatriz and Ana María, on the occasion of their 12th and 25th birthdays.

Permissions

Rutherfordine. Part of **Figure 2** and data contained in **Table 1** adapted from Ref. [99] with permission from American Chemical Society, Copyright (2017). Part of **Figure 3** adapted from Ref. [102] with permission from American Chemical Society, Copyright (2018). Parts of **Figures 4–6** adapted from Ref. [103] with permission from American Chemical Society, Copyright (2018).

Gamma uranium trioxide. Part of **Figure 2** and data contained in **Table 1** adapted from Ref. [100] with permission from American Chemical Society, Copyright (2017). Part of **Figure 3** adapted from Ref. [102] with permission from American Chemical Society, Copyright (2018). Parts of **Figures 4–6** adapted from Ref. [103] with permission from American Chemical Society, Copyright (2018).

Dehydrated schoepite, studtite, metastudtite, and soddyite. Data contained in **Table 1** adapted from Ref. [102] with permission from American Chemical Society, Copyright (2018). Parts of **Figures 4–6** adapted from Ref. [103] with permission from American Chemical Society, Copyright (2018).

Schoepite and metaschoepite. Parts of **Figures 2–6** and data contained in **Tables 1 and 2** adapted from Ref. [104] with permission from American Chemical Society.

Becquerelite. Part of **Figures 4–6** and data contained in **Tables 1** and **2** reproduced from Ref. [105] with permission from the Royal Society of Chemistry.

Author details

Francisco Colmenero Ruiz

Address all correspondence to: francisco.colmenero@iem.cfmac.csic.es

Instituto de Estructura de la Materia – Consejo Superior de Investigaciones Científicas (IEM-CSIC), Madrid, Spain

References

[1] Guggenheim EA. Thermodynamics: An Advanced Treatment for Chemists and Physicists. Amsterdam: North-Holland; 1967. ISBN: 0444869514

[2] Gorman-Lewis D, Burns PC, Fein JB. Review of uranyl mineral solubility measurements. Journal of Chemical Thermodynamics. 2008;**40**:335-352. DOI: 10.1016/j.jct.2007.12.004

[3] Shvareva TY, Fein JB, Navrotsky A. Thermodynamic properties of uranyl minerals: Constraints from calorimetry and solubility measurements. Industrial and Engineering Chemical Research. 2012;**51**:607-613. DOI: 10.1021/ie2002582

[4] Gasparik T. An internally consistent thermodynamic model for the system CaO–MgO–Al_2O_3–SiO_2 derived primarily from phase equilibrium data. The Journal of Geology. 2000;**108**:103-119. DOI: 10.1086/314389

[5] Bruno J, Bosbach D, Kulik D, Navrotsky A. Chemical thermodynamics of solid solutions of interest in radioactive waste management. In: Mompean FJ, Illemassene M, editors. Issy-Les-Moulineaux, France: OECD Nuclear Energy Agency, Data Bank; 2007. DOI: 10.1787/9789264033191-en

[6] Chopelas A. Thermal properties of forsterite at mantle pressures derived from vibrational spectroscopy. Physics and Chemistry of Minerals. 1990;**17**:149-156. DOI: 10.1007/BF00199666

[7] Chopelas A. Thermal expansion, heat capacity, and entropy of MgO at mantle pressures. Physics and Chemistry of Minerals. 1990;**17**:142-148. DOI: 10.1007/BF00199665

[8] Hofmeister AM, Chopelas A. Thermodynamic properties of pyrope and grossular from vibrational spectroscopy. American Mineralogist. 1991;**76**:880-891. ISSN: 0003-004X

[9] Helgeson HC, Delany JM, Nesbit HW, Bird DK. Summary and critique of the thermodynamic properties of rock-forming minerals. American Journal of Science. 1978;**278A**:1-229. ISSN: 0002-9599

[10] Wagman DD, Evans WH, Parker VB, Schumm RH, Halow I, et al. The NBS tables of chemical thermodynamic properties. Selected values for inorganic and C1 and C2 organic substances in SI units. Journal of Physical Chemistry Reference Data. 1982;**11** (Suppl. 2):1-392. ISBN: 0-88318-417-6

[11] Chase MW, Davies CA, Downey JR, Frurip DJ, McDonald RA, Syverud AN. JANAF Thermochemical Tables. Third Edition. Journal of Physical Chemistry Reference Data. 1985;**14**(Suppl. 1):1-1856. ISBN: 0-88318-473-7

[12] Barin I. Thermochemical Data of Pure Substances. Third ed. Weinheim: VCH; 1995. DOI: 10.1002/9783527619825

[13] Barin I, Schmidt W, Schilling J. EQUITHERM Database and Software Package for Chemical Equilibrium Calculations on Personal Computers. Munster: VCH Scientific Software; 1993. ISBN: 352726373X

[14] Berman RG. Internally-consistent thermodynamic data for minerals in the system Na_2O-K_2O-CaO-MgO-FeO-Fe_2O_3-Al_2O_3-SiO_2-TiO_2-H_2O-CO_2. Journal of Petrology. 1988;**29**: 445-522. DOI: 10.1093/petrology/29.2.445

[15] Holland TJB, Powell R. An enlarged and updated internally consistent thermodynamic dataset with uncertainties and correlations: The system K_2O-Na_2O-CaO-MgO-MnO-FeO-Fe_2O_3-Al_2O_3-TiO_2-SiO_2-C-H_2-O_2. Journal of Metamorphic Geology. 1990;**8**:89-124. DOI: 10.1111/j.1525-1314.1990.tb00458.x

[16] Holland TJB, Powell R. An internally consistent thermodynamic data set for phases of petrological interest. Journal of Metamorphic Geology. 1998;**16**:309-343. DOI: 10.1111/j.1525-1314.1998.00140.x

[17] Holland TJB, Powell R. An improved and extended internally consistent thermodynamic dataset for phases of petrological interest, involving a new equation of state for solids. Journal of Metamorphic Geology. 2011;**29**:333-383. DOI: 10.1111/j.1525-1314.2010.00923.x

[18] Bale CW, Belisle E, Chartrand P, Decterov SA, Eriksson G, Gheribi AE, et al. FactSage thermochemical software and databases, 2010–2016. Calphad. 2016;**54**:35-53. DOI: 10.1016/j.calphad.2016.05.002

[19] Lukas HL, Henig ET, Zimmermann B. Optimization of phase diagrams by a least squares method using simultaneously different types of data. Calphad. 1977;**1**:225-236. DOI: 10.1016/0364-5916(77)90002-5

[20] Van de Walle A, Ceder G. Automating first-principles phase diagram calculations. Journal of Phase Equilibria. 2002;**23**:348-359. DOI: 10.1361/10549710277

[21] Fabrichnaya O, Saxena SK, Richet P, Westrum EF. Thermodynamic Data, Models, and Phase Diagrams in Multicomponent Oxide Systems. Berlin: Springer-Verlag; 2004. ISBN: 3540140182

[22] Eriksson G. Thermodynamic studies of high-temperature equilibria. XII. SOLGASMIX, a computer-program for calculation of equilibrium compositions in multiphase systems. Chemica Scripta. 1975;**8**:100-103. ISSN: 0004-2056

[23] George B, Brown LP, Farmer CH, Buthod P, Manning FS. Computation of multicomponent, multiphase equilibrium. Industrial and Engineering Chemical Process Design and Development. 1976;**15**:372-377. DOI: 10.1021/i260059a003

[24] Smith WR, Missen RW. Chemical Reaction Equilibrium Analysis: Theory and Algorithms. New York: Wiley-Interscience; 1982. ISBN: 0471093475

[25] Harvie CE, Greenberg JP, Weare JH. A chemical equilibrium algorithm for highly non-ideal multiphase systems: Free energy minimization. Geochimica et Cosmochimica Acta. 1987;**51**:1045-1057. DOI: 10.1016/0016-7037(87)90199-2

[26] Piro MHA, Simunovic S. Performance enhancing algorithms for computing thermodynamic equilibria. Calphad. 2012;**39**:104-110. DOI: 10.1016/j.calphad.2012.09.005;

[27] Piro MHA, Simunovic S. Global optimization algorithms to compute thermodynamic equilibria in large complex systems with performance considerations. Computational Material Science. 2016;**118**:87-96. DOI: 10.1016/j.commatsci.2016.02.043

[28] Piro MHA. Updating the estimated assemblage of stable phases in a Gibbs energy minimizer. Calphad. 2017;**58**:115-121. DOI: 10.1016/j.calphad.2017.06.002

[29] Sundman B, Jansson B, Andersson JO. The thermo-calc databank system. Calphad. 1985; **9**:153-190. DOI: 10.1016/0364-5916(85)90021-5

[30] Eriksson G, Hack K. ChemSage—A computer program for the calculation of complex chemical equilibria. Metal Transactions B. 1990:**21**;1013-1023. DOI: 10.1007/BF02670272.

[31] Piro MHA, Simunovic S, Besmann TM, Lewis BJ, Thompson WT. The thermochemistry library Thermochimica. Computational Materials Science. 2013;**67**:266-272. DOI: 10.1016/j.commatsci.2012. 09.011

[32] Miron GD, Kulik DA, Dmytrieva SV, Wagner T. GEMSFITS: Code package for optimization of geochemical model parameters and inverse modeling. Applied Geochemistry. 2015;**55**:28-45. DOI: 10.1016/j.apgeochem.2014.10.013

[33] Saxena SK, Eriksson G. Theoretical computation of mineral assemblages in pyrolite and lherzolite. Journal of Petrology. 1983;**24**:538-555. DOI: 10.1093/petrology/24.4.538

[34] Saxena SK, Eriksson G. High temperature phase equilibria in a solar-composition gas. Geochimica et Cosmochimica Acta. 1983;**47**:1865-1874. DOI: 10.1016/0016-7037(83)90203-X

[35] Saxena SK, Eriksson G. Low- to medium-temperature phase equilibria in a gas of solar composition. Earth and Planetary Science Letters. 1983;**65**:7-16

[36] Saxena SK, Eriksson G. Chemistry of formation of terrestrial planets. Advances in Physical Geochemistry. 1986;**6**:30-101. DOI: 10.1016/0012-821X(83)90185-1

[37] Hemingway BS. Thermodynamic Properties of Selected Uranium Compounds and Aqueous Species at 298.15 K and 1 Bar and at Higher Temperatures—Preliminary Models for the Origin of Coffinite Deposits. USGS Open-File Report 82–619; 1982. Available from: https://pubs.usgs.gov/of/1982/0619/report.pdf [Accessed: 2018-05-15]

[38] Langmuir D. Aqueous Environmental Geochemistry. New Jersey: Prentice-Hall; 1997. pp. 486-557. ISBN: 0023674121

[39] Casas I, Bruno J, Cera E, Finch RJ, Ewing RC. Kinetic and Thermodynamic Studies of Uranium Minerals Assessment of the Long-Term Evolution of Spent Nuclear Fuel. SKB Technical Report 94–16. Stockholm: Swedish Nuclear Fuel and Waste Management Co.; 1994. Available from: http://www.skb.com/publication/10579/TR94-16webb.pdf [Accessed: 2018-05-15]

[40] Navrotsky A, Shvareva TY, Guo X, Rock PA. Chapter 5: Thermodynamics of Uranium Minerals and Related Materials. In: Burns PC, Sigmon GE, editors. Uranium – Cradle to Grave. Mineralogical Association of Canada Short Course 43. Mineralogical Association of Canada: Québec; 2013. ISBN: 0921294530

[41] Sassani DC, Jové-Colón CF, Weck PF, Jerden JL, Frey KE, Cruse T, Ebert WL, Buck EC, Wittman RS. Used Fuel Degradation: Experimental and Modeling Report. Fuel Cycle

Research and Development Report FCRD-UFD-2013-000404. Sandia National Laboratories: Albuquerque, New Mexico; 2013. Available from: https://www.energy.gov/ne/downloads/used-fuel-degradation-experimental-and-modeling-report [Accessed: 2018-05-15]

[42] Frondel C. Mineral composition of gummite. American Mineralogist. 1956;**41**:539-568. ISSN: 0003-004X

[43] Frondel C. Systematic mineralogy of uranium and thorium. U.S. Geological Survey Bulletin. 1958;**1064**:1-400. Available from: http://pubs.er.usgs.gov/publication/b1064ER [Accessed: 2018-05-15]

[44] Finch RJ, Ewing RC. The corrosion of uraninite under oxidizing conditions. Journal of Nuclear Materials. 1992;**190**:133-156. DOI: 10.1016/0022-3115(92)90083-W

[45] Pearcy EC, Prikryl JD, Murphy WM, Leslie BW. Alteration of uraninite from the Nopal I deposit, Peña Blanca District, Chihuahua, Mexico, compared to degradation of spent nuclear fuel in the proposed US high-level nuclear waste repository at Yucca Mountain, Nevada. Applied Geochemistry. 1994;**9**:713-732. DOI: 10.1016/0883-2927(94)90030-2

[46] Wronkiewicz DJ, Bates JK, Gerding TJ, Veleckis E, Tani BS. Uranium release and secondary phase formation during unsaturated testing of UO_2 at 90°C. Journal of Nuclear Materials. 1992;**190**:107-127. DOI: 10.1016/0022-3115(92)90081-U

[47] Wronkiewicz DJ, Bates JK, Wolf SF, Buck EC. Ten-year results from unsaturated drip tests with UO2 at 90°C: Implications for the corrosion of spent nuclear fuel. Journal of Nuclear Materials. 1996;**238**:78-95. DOI: 10.1016/S0022-3115(96)00383-2

[48] Finch RJ, Murakami T. Systematics and paragenesis of uranium minerals. In: Ribbe PH, editor. URANIUM: Mineralogy, Geochemistry and the Environment; Reviews in Mineralogy, Vol. 38. New York: Mineralogical Society of America; 1999. pp. 91-180. ISBN: 0-939950-50-2

[49] Clark DL, Hobart DE, Neu MP. Actinide carbonate complexes and their importance in actinide environmental chemistry. Chemical Reviews. 1995;**95**:25-48. DOI: 10.1021/cr00033a002

[50] Sattonnay G, Ardois C, Corbel C, Lucchini JF, Barthe MF, Garrido F, Gosset D. Alpha-radiolysis effects on UO_2 alteration in water. Journal of Nuclear Materials. 2001;**288**:11-19. DOI: 10.1016/S0022-3115(00)00714-5

[51] Kubatko KA, Helean KB, Navrotsky A, Burns PC. Stability of peroxide-containing uranyl minerals. Science. 2003;**302**:1191-1193. DOI: 10.1126/science.1090259

[52] Kubatko KA. Crystallography, hierarchy of crystal structures, and chemical thermodynamics of selected uranyl phases [PhD thesis]. Illinois: Graduate School of the University of Notre Dame; 2005. Available from: https://www.researchgate.net/publication/277794995_Crystallography_Hierarchy_of_Crystal_Structures_and_Chemical_Thermodynamics_of_Select_Uranyl_Phases [Accessed: 2018-05-15]

[53] Guo X, Ushakova SV, Labs S, Curtius H, Bosbach D, Navrotsky A. Energetics of metastudtite and implications for nuclear waste alteration. Proceedings of the National Academy of Sciences of the United States of America. 2014;**111**:17737-17742. DOI: 10.1073/pnas.1421144111

[54] Armstrong CR, Nyman M, Shvareva TY, Sigmon GE, Burns PC, Navrotsky A. Uranyl peroxide enhanced nuclear fuel corrosion in seawater. Proceedings of the National Academy of Sciences of the United States of America. 2012;**109**:1874-1877. DOI: 10.1073/pnas.1119758109

[55] Burns PC, Ewing RC, Miller ML. Incorporation mechanisms of actinide elements in to the structures of U6+ phases formed during the oxidation of spent nuclear fuel. Journal of Nuclear Materials. 1997;**245**:1-9. DOI: 10.1016/S0022-3115(97)00006-8

[56] Burns PC. The crystal chemistry of uranium. In: Ribbe PH, editor. URANIUM: Mineralogy, Geochemistry and the Environment; Reviews in Mineralogy, Vol. 38. New York: Mineralogical Society of America; 1999. pp. 23-90. ISBN: 0-939950-50-2

[57] Burns PC. U6+ minerals and inorganic compounds: Insights into an expanded structural hierarchy of crystal structures. The Canadian Mineralogist. 2005;**43**:1839-1894. DOI: 10.2113/gscanmin.43.6.1839

[58] Burns PC. The structure of Boltwoodite and implications of solid solution towards sodium Boltwoodite. The Canadian Mineralogist. 1998;**36**:1069-1075. ISSN: 0008-4476

[59] Burns PC. Cs Boltwoodite obtained by ion exchange from single crystals: Implications for radionuclide release in a nuclear repository. Journal of Nuclear Materials. 1999;**265**:218-223. DOI: 10.1016/S0022-3115(98)00646-1

[60] Burns PC, Li Y. The structures of becquerelite and Sr-exchanged becquerelite. American Mineralogist. 2002;**87**:550-557. DOI: 10.2138/am-2002-0418

[61] Klingensmith AL, Burns PC. Neptunium substitution in synthetic Uranophane and Soddyite. American Mineralogist. 2007;**92**:1946-1951. DOI: 10.2138/am.2007.2542

[62] Burns PC, Deely KM, Skanthakumar S. Neptunium incorporation into uranyl compounds that form as alteration products of spent nuclear fuel: Implications for geologic repository performance. Radiochimica Acta. 2004;**92**:151-159. DOI: 10.1524/ract.92.3.151.30491

[63] Burns PC, Miller ML, Ewing RC. U6+ minerals and inorganic phases: A comparison and hierarchy of crystal structures. The Canadian Mineralogist. 1996;**34**:845-880. ISSN: 0008-4476

[64] Burns PC, Ewing RC, Hawthorne FC. The crystal chemistry of hexavalent uranium: Polyhedron geometries, bond-valence parameters, and polymerization of polyhedra. The Canadian Mineralogist. 1997;**35**:1551-1570. ISSN: 0008-4476

[65] Douglas M, Clark SB, Utsunomiya S, Ewing RC. Cesium and strontium incorporation into uranophane, $Ca[(UO_2)(SiO_3OH)]_2 \cdot 5H_2O$. Journal of Nuclear Science and Technology Supplement. 2002;**3**:504-507. DOI: 10.1080/00223131.2002.10875517

[66] Douglas M, Clark SB, Friese JI, Arey BW, Buck EC, Hanson BD, Utsunomiya S, Ewing RC. Microscale characterization of uranium(VI) silicate solids and associated neptunium(V). Radiochimica Acta. 2005;**93**:265-272. DOI: 10.1524/ract.93.5.265.64281

[67] Murphy WM, Grambow B. Thermodynamic interpretation of neptunium coprecipitation in uranophane for application to the Yucca Mountain repository. Radiochimica Acta. 2008;**96**:563-567. DOI: 10.1524/ract.2008.1537

[68] Shuller LC, Ewing RC, Becker U. Quantum-mechanical evaluation of Np-incorporation into studtite. American Mineralogist. 2010;**95**:1151-1160. ISSN: 0003-004X

[69] Shuller LC, Ewing RC, Becker U. Np-incorporation into uranyl phases: A quantum–mechanical evaluation. Journal of Nuclear Materials. 2013;**434**:440-450. DOI: 10.1016/j.jnucmat.2011.04.016

[70] Shuller LC, Bender WM, Walker SM, Becker U. Quantum-mechanical methods for quantifying incorporation of contaminants in proximal minerals. Minerals. 2014;**4**:690-715. DOI: 10.3390/min4030690

[71] Gorman-Lewis D, Mazeina L, Fein JB, Szymanowski JES, Burns PC, Navrotsky A. Thermodynamic properties of soddyite from solubility and calorimetry measurements. Journal of Chemical Thermodynamics. 2007;**39**:568-575. DOI: 10.1016/j.jct.2006.09.005

[72] Grenthe I, Fuger J, Konings RJM, Lemire RJ, Muller AB, Nguyen-Trung C, Wanner H. Chemical Thermodynamics of Uranium. Issy-Les-Moulineaux, France: Nuclear Energy Agency Organisation for Economic Co-Operation and Development, OECD; 2004. Available from: https://oecd-nea.org/dbtdb/pubs/uranium.pdf [Accessed: 2018-05-15]

[73] Guillaumont NYR, Fanghänel T, Neck V, Fuger J, Palmer DA, Grenthe I, Rand MH. In: Mompean FJ, Illemassene M, Domenech-Orti C, Ben Said K, editors. Update on the Chemical Thermodynamics of Uranium, Neptunium, Plutonium, Americium, and Technetium. Issy-Les-Moulineaux, France: OECD Nuclear Energy Agency, Data Bank; 2003. Available from: https://www.oecd-nea.org/dbtdb/pubs/vol5-update-combo.pdf [Accessed: 2018–05-15]

[74] Chevalier PY, Fischer E, Cheynet B. Progress in the thermodynamic modelling of the O–U binary system. Journal of Nuclear Materials. 2002;**303**:1-28. DOI: 10.1016/S0022-3115(02)00813-9

[75] Konings RJM, Benes O, Kovacs A, Manara D, Gorokhov DS, Iorish VS, Yungman V, Shenyavskaya E, Osina E. The thermodynamic properties of the f-elements and their compounds. Part 2. The lanthanide and actinide oxides. Journal of Physical and Chemical Reference Data. 2014;**43**:013101. DOI: 10.1063/1.4825256

[76] Wanner H, Forest I, editors. Chemical Thermodynamics of Uranium. Amsterdam: Elsevier Science Publishers B.V; 1992. ISBN: 9780444893819

[77] Murphy WM, Pabalan RT. Review of Empirical Thermodynamic Data for Uranyl Silicate Minerals and Experimental Plan. Nuclear Regulatory Commission Contract NRC-02-93-005.

San Antonio, Texas: Center for Nuclear Waste Regulatory Analyses; 1995. Available from: https://www.nrc.gov/docs/ML0402/ML040210708.pdf [Accessed: 2018-05-15]

[78] Kubatko KA, Helean KB, Navrotsky A, Burns PC. Thermodynamics of uranyl minerals: Enthalpies of formation of rutherfordine, UO_2CO_3, andersonite, $Na_2CaUO_2(CO_3)_3(H_2O)_5$, and grimselite, $K_3Na(UO_2)(CO_3)\cdot 3H_2O$. American Mineralogist. 2005;**90**:1284-1290. DOI: 10.2138/am.2005.1821

[79] Gorman-Lewis D, Shvareva TY, Kubatko KA, Burns PC, Wellman DM, McNamara B, Szymanowsky JES, Navrotsky A, Fein JB. Thermodynamic properties of autunite, uranyl hydrogen phosphate, and uranyl orthophosphate from solubility and calorimetric measurements. Environmental Science and Technology. 2009;**43**:7416-7422. DOI: 10.1021/es9012933

[80] Nguyen SN, Silva RJ, Weed HC, Andrews LE. Standard Gibbs free energies of formation at the temperature 303.15 K of four uranyl silicates: Soddyite, uranophane, sodium Boltwoodite, and sodium Weeksite. Journal of Chemical Thermodynamics. 1992;**24**:259-276. DOI: 10.1016/S0021-9614(05)80155-7

[81] Prikryl JD. Uranophane dissolution and growth in $CaCl_2$–SiO_2(aq) test solutions. Geochimica et Cosmochimica Acta. 2008;**72**:4508-4520. DOI: 10.1016/j.gca.2008.06.022

[82] Shvareva TY, Mazeina L, Gorman-Lewis D, Burns PC, Szymanowski JES, Fein JB, Navrotsky A. Thermodynamic characterization of Boltwoodite and uranophane: Enthalpy of formation and aqueous solubility. Geochimica et Cosmochimica Acta. 2011; **75**:5269-5282. DOI: 10.1016/j.gca.2011.06.041

[83] Szenknect S, Mesbah A, Cordara T, Clavier N, Brau HP, Le Goffa X, Poinssot C, Ewing RC, Dacheux N. First experimental determination of the solubility constant of coffinite. Geochimica et Cosmochimica Acta. 2016;**81**:36-53. DOI: 10.1016/j.gca.2016.02.010

[84] Guo X, Szenknect S, Mesbah A, Labs S, Clavier N, Poinssot C, Ushakova SV, Curtius H, Bosbach D, Ewing RC, Burns PC, Dacheux N, Navrotsky A. Thermodynamics of formation of coffinite, $USiO_4$. Proceedings of the National Academy of Sciences of the United States of America. 2014;**112**:6551-6555

[85] Gueneau C, Baichi M, Labroche D, Chatillon CB, Sundman B. Thermodynamic assessment of the uranium–oxygen system. Journal of Nuclear Materials. 2002;**304**:161-175. DOI: 10.1016/S0022-3115(02)00878-4

[86] Loukusa H, Ikonen T, Valtavirta V, Tulkki V. Thermochemical modeling of nuclear fuel and the effects of oxygen potential buffers. Journal of Nuclear Materials. 2016;**481**:101-110. DOI: 10.1016/j.jnucmat.2016.09.014

[87] Piro MHA, Besmann TM, Simunovic S, Lewis BJ, Thompson WT. Numerical verification of equilibrium thermodynamic computations in nuclear fuel performance codes. Journal of Nuclear Materials. 2011;**414**:399-407. DOI: 10.1016/j.jnucmat.2011.05.012

[88] Piro MHA, Banfield J, Clarno KT, Thompson WT. Coupled thermochemical, isotopic evolution and heat transfer simulations in highly irradiated UO_2 nuclear fuel. Journal of Nuclear Materials. 2013;**441**:240-251

[89] Piro MHA, Banfield J, Clarno KT, Simunovic S, Besmann TM. Simulation of thermochemistry and isotopic evolution of irradiated nuclear fuel. Transactions of the American Nuclear Society. 2013;**108**:367-370. ISSN: 0003-018X

[90] Piro MHA, Leitch BW. Conjugate heat transfer simulations of advanced research reactor fuel. Nuclear Engineering and Design. 2014;**274**:30-43. DOI: 10.1016/j.nucengdes.2014.03.054

[91] Corcoran EC, Lewis BJ, Thompson WT, Mouris J, He Z. Controlled oxidation experiments of simulated irradiated UO_2 fuel in relation to thermochemical modelling. Journal of Nuclear Materials. 2011;**414**:73-82. DOI: 10.1016/j.jnucmat.2010.11.063

[92] Corcoran EC, Kaye MH, Piro MHA. An overview of thermochemical modelling of CANDU fuel and applications to the nuclear industry. Calphad. 2016;**55**:52-62. DOI: 10.1016/j.calphad.2016.04.010

[93] Besmann TM, Bartel TJ, Bertolus M, Blanc V, Bouineau V, Carlot G, et al. State-of-the-Art Report on Multi-Scale Modelling of Nuclear Fuels. Nuclear Science NEA/NSC/R/(2015)5. Nuclear Energy Agency—Energy Agency Organisation for Economic Co-operation and Development; 2015. Available from: https://www.oecd-nea.org/science/docs/2015/nsc-r2015-5.pdf [Accessed: 2018-05-15]

[94] Besmann TM, McMurray JW, Simunovic S. Application of thermochemical modeling to assessment/evaluation of nuclear fuel behavior. Calphad. 2016;**55**:47-51. DOI: 10.1016/j.calphad.2016.04.004

[95] Smith AL, Gueneau C, Fleche JL, Chatain S, Benes O, Konings RJM. Thermodynamic assessment of the Na-O and Na-U-O systems: Margin to the safe operation of SFRs. Journal of Chemical Thermodynamics. 2017;**114**:93-115. DOI: 10.1016/j.jct.2017.04.003

[96] Weck PF, Kim E. Layered uranium(VI) hydroxides: Structural and thermodynamic properties of dehydrated schoepite α-$UO_2(OH)_2$. Dalton Transactions. 2014;**43**:17191-17199. DOI: 10.1039/C4DT02455A

[97] Weck PF, Kim E. Uncloaking the thermodynamics of the studtite to metastudtite shear-induced transformation. Journal of Physical Chemistry C. 2016;**120**:16553-16560. DOI: 10.1021/acs.jpcc.6b05967

[98] Beridze G, Kowalski PM. Benchmarking the DFT+U method for thermochemical calculations of uranium molecular compounds and solids. Journal of Physical Chemistry A. 2014;**118**:11797-11810. DOI: 10.1021/jp5101126

[99] Colmenero F, Bonales LJ, Cobos J, Timón V. Thermodynamic and mechanical properties of rutherfordine mineral based on density functional theory. Journal of Physical Chemistry C. 2017;**121**:5994-6001. DOI: 10.1021/acs.jpcc.7b00699

[100] Colmenero F, Bonales LJ, Cobos J, Timón V. Density functional theory study of the thermodynamic and Raman vibrational properties of γ-UO_3 polymorph. Journal of Physical Chemistry C. 2017;**121**:14507-14516. DOI: 10.1021/acs.jpcc.7b04389

[101] Colmenero F. Characterization of secondary phases of spent nuclear fuel under final geological disposal conditions [PhD thesis]. Madrid: Universidad Autónoma de Madrid; 2017. 443 pp. DOI: 10.13140/RG.2.2.10526.43843

[102] Colmenero F, Fernández AM, Cobos J, Timón V. Thermodynamic properties of uranyl-containing materials based on density functional theory. Journal of Physical Chemistry C. 2018;**122**:5254-5267. DOI: 10.1021/acs.jpcc.7b12341

[103] Colmenero F, Fernández AM, Cobos J, Timón V. Temperature-dependent Gibbs free energies of reaction of uranyl-containing materials based on density functional theory. Journal of Physical Chemistry C. 2018;**122**:5268-5279. DOI: 10.1021/acs.jpcc.7b12368

[104] Colmenero F, Fernández AM, Cobos J, Timón V. Periodic DFT study of the thermodynamic properties and stability of schoepite and metaschoepite mineral phases. ACS Earth and Space Chemistry. 2018; Under review

[105] Colmenero F, Fernández AM, Cobos J, Timón V. Becquerelite mineral phase: Crystal structure and thermodynamic and mechanic stability by using periodic DFT. RSC Advances. 2018;**8**:24599-24616. DOI: 10.1039/c8ra04678f

[106] Benedict M, Pigford TH, Levi HW. Nuclear Chemical Engineering. New York: McGraw-Hill; 1981. ISBN: 0070045313

[107] Schulz WW. Uranium Processing; in Encyclopedia Britannica. Available from: https://global.britannica.com/technology/uranium-processing [Accessed: 2018-05-15]

[108] McNamara B, Buck EC, Hanson B. Observation of studtite and metastudtite on spent fuel. MRS Online Proceedings Library. 2002;**757**:401-406. DOI: 10.1557/PROC-757-II9.7

[109] Hanson BD, McNamara B, Buck EC, Friese JI, Jenson E, Krupka K, Arey BW. Corrosion of commercial spent nuclear fuel. 1. Formation of studtite and metastudtite. Radiochimica Acta. 2005;**93**:159-168. DOI: 10.1524/ract.93.3.159.61613

[110] Forbes TZ, Horan P, Devine T, McInnis D, Burns PC. Alteration of dehydrated schoepite and soddyite to studtite, $[(UO_2)O_2(H_2O)_2](H_2O)_2$. American Mineralogist. 2011;**96**:202-206. DOI: 10.2138/am.2011.3517

[111] Weck PF, Kim E, Jové-Colón CF, Sassani DC. Structures of uranyl peroxide hydrates: A first-principles study of studtite and metastudtite. Dalton Transactions. 2012;**41**:9748-9752. DOI: 10.1039/C2DT31242E

[112] Abrefah J, Marschmann S, Jenson ED. Examination of the Surface Coatings Removed from K-East Basin Fuel Elements. Report of the U.S. Department of Energy, Pacific Northwest National Laboratory PNNL-11806. US-DOE: Richland, Washington; 1998

[113] Schmidt AJ, Delegard CH. Assessment of K Basin Sludge Volume Expansion Resulting from Uranium Corrosion during Storage. Report of the U.S. Department of Energy, Pacific Northwest National Laboratory PNNL-13786. US-DOE: Richland, Washington; 2002

[114] Delegard CH, Schmid AJ. Uranium Metal Reaction Behavior in Water, Sludge, and Grout. Report of the U.S. Department of Energy, Pacific Northwest National Laboratory PNNL-17815. US-DOE: Richland, Washington; 2008

[115] Delegard CH, Schmidt AJ, Chenault JW. Mechanical Properties of K Basin Sludge Constituents and their Surrogates. Report of the U.S. Department of Energy, Pacific Northwest National Laboratory PNNL-14947. US-DOE: Richland, Washington; 2004

[116] Cantrell KJ, Krupka KM, Deutsch WJ, Lindberg MJ. Residual waste from Hanford tanks 241-C-203 and 241-C-204. 2. Contaminant release model. Environmental Science and Technology. 2006;**40**:3755-3761. DOI: 10.1021/es0511568

[117] Burakov BE, Strykanova EE, Anderson EB. Secondary uranium minerals on the surface of Chernobyl "lava". MRS Online Proceedings. Library. 1997;**465**:1309-1311. DOI: 10.1557/PROC-465-1309

[118] Grenthe I, Drozdzynski J, Fujino T, Buck EC, Albrecht-Schmitt TE, Wolf SF. Uranium. In: Morss LR, Edelstein NM, Fuger J, editors. The Chemistry of Actinide and Transactinide Elements. Vol. I. Berlin: Springer Science and Business Media; 2006. pp. 253-638. ISBN 978-94-007-0211-0, Chapter V

[119] Plasil J. Oxidation-hydration weathering of uraninite: The current state-of knowledge. Journal of Geosciences. 2014;**59**:99-114. DOI: 10.3190/jgeosci.163

[120] Colmenero F, Bonales LJ, Cobos J, Timón V. Study of the thermal stability of studtite by in situ Raman spectroscopy and DFT calculations. Spectrochimica Acta. A. 2017;**174**:245-253. DOI: 10.1016/j.saa.2016.11.040

[121] Bonales LJ, Colmenero F, Cobos J, Timón V. Spectroscopic Raman characterization of rutherfordine: A combined DFT and experimental study. Physical Chemistry Chemical Physics. 2016;**18**:16575-16584. DOI: 10.1039/C6CP01510G

[122] Colmenero F, Bonales LJ, Cobos J, Timón V. Structural, mechanical and vibrational study of uranyl silicate mineral soddyite by DFT calculations. Journal of Solid State Chemistry. 2017;**253**:249-257. DOI: 10.1016/j.jssc.2017.06.002

[123] Colmenero F, Cobos J, Timón V. Periodic DFT study of the structure, Raman spectrum and mechanical properties of schoepite mineral. Inorganic Chemistry. 2018;**57**:4470-4481. DOI: 10.1021/acs.inorgchem.8b00150

[124] Payne MC, Teter MP, Ailan DC, Arias A, Joannopoulos JD. Iterative minimization techniques for ab initio total-energy calculations: Molecular dynamics and conjugate gradients. Review of Modern Physics. 1992;**64**:1045-1097. DOI: 10.1103/RevModPhys.64.1045

[125] Perdew JP, Burke K, Ernzerhof M. Generalized gradient approximation made simple. Physical Review Letters. 1996;**77**:3865-3868. DOI: 10.1103/PhysRevLett.77.3865

[126] Grimme S. Semiempirical GGA-type density functional constructed with a long-range dispersion correction. Journal of Computational Chemistry. 2006;**27**:1787-1799. DOI: 10.1002/jcc.20495

[127] Perdew JP, Ruzsinszky A, Csonka GI, Vydrov OA, Scuseria GE, Constantin LA, Zhou X, Burke K. Restoring the density-gradient expansion for exchange in solids and surfaces. Physical Review Letters. 2008;**100**:136406. DOI: 10.1103/PhysRevLett.100.136406

[128] Weck PF, Gordon ME, Greathouse JA, Bryan CR, Meserole SP, Rodriguez MA, Payne C, Kim E. Infrared and Raman spectroscopy of α-ZrW2O8: A comprehensive density functional perturbation theory and experimental study. Journal of Raman Spectroscopy. 2018; **48**:1373-1384. DOI: 10.1002/jrs.5396

[129] Weck PF, Kim E, Greathouse JA, Gordon ME, Bryan CR. Assessing exchange-correlation functionals for elasticity and thermodynamics of α-ZrW2O8: A density functional perturbation theory study. Chemical Physics Letters. 2018;**658**:195-199. DOI: 10.1016/j.cplett.2018.03.025

[130] Csonka GI, Perdew JP, Ruzsinszky A, Philipsen PHT, Lebègue S, Paier J, Vydrov OA, Ángyán JG. Assessing the performance of recent density functionals for bulk solids. Physical Review B. 2009;**79**:155107. DOI: 10.1103/PhysRevB.79.155107

[131] Clark SJ, Segall MD, Pickard CJ, Hasnip PJ, Probert MIJ, Refson K, Payne MC. First principles methods using CASTEP. Zeitschrift für Kristallographie-Crystalline Materials. 2005;**220**:567-570. DOI: 10.1524/zkri.220.5.567.65075

[132] Materials Studio. Available from: http://accelrys.com/products/collaborativescience/biovia-materials-studio/ [Accessed: 2018-04-30]

[133] Troullier N, Martins JL. Efficient pseudopotentials for plane-wave calculations. Physical Review B. 1991;**43**:1993-2006. DOI: 10.1103/PhysRevB.43.1993

[134] Pfrommer BG, Cote M, Louie MSG, Cohen ML. Relaxation of crystals with the quasi-Newton method. Journal of Computational Physics. 1997;**131**:233-240. DOI: 10.1006/jcph.1996.5612

[135] Monkhorst HJ, Pack JD. Special points for Brillouin-zone integration. Physical Review B. 1976;**13**:5188-5192. DOI: 10.1103/PhysRevB.13.5188

[136] Downs RT, Bartelmehs KL, Gibbs GV, Boisen MB. Interactive software for calculating and displaying X-ray or neutron powder diffractometer patterns of crystalline materials. American Mineralogist. 1993;**78**:1104-1107. ISSN: 0003-004X

[137] Baroni S, de Gironcoli S, Dal Corso SA. Phonons and related crystal properties from density-functional perturbation theory. Review of Modern Physics. 2001;**73**:515-562. DOI: 10.1103/RevModPhys.73.515

[138] Gonze X, Lee C. Dynamical matrices, born effective charges, dielectric permittivity tensors, and Interatomic force constants from density-functional perturbation theory. Physical Review B. 1997;**55**:10355-10368. DOI: 10.1103/PhysRevB.55.10355

[139] Refson K, Tulip PR, Clark SJ. Variational density-functional perturbation theory for dielectrics and lattice dynamics. Physical Review B. 2006;**73**:155114. DOI: 10.1103/PhysRevB.73.155114

[140] Lee C, Gonze X. Ab initio calculation of the thermodynamic properties and atomic temperature factors of SiO_2 α-quartz and stishovite. Physical Review B. 1995;**51**:8610-8613. DOI: 10.1103/PhysRevB.51.8610

[141] Gurevich VM, Sergeyeva EI, Gavrichev KS, Gorbunov VE, Khodakovsky IL. Low-temperature specific heat of UO_2CO_3. Russian Journal of Physical Chemistry. 1987;**61**: 856-857. ISSN: 0036-0244

[142] Cordfunke EHP, O'Hare PAG. The Chemical Thermodynamics of Actinide Elements and Compounds. Part 3. Miscellaneous Actinide Compounds. Vienna, Austria: International Atomic Energy Agency; 1978. Online Computer Library Center (OCLC) number: 150463669

[143] Cordfunke EHP, Westrum EF. The thermodynamic properties of β-UO_3 and γ-UO_3. Thermochimica Acta. 1988;**124**:285-296. DOI: 10.1016/0040-6031(88)87031-X

[144] Jones WM, Gordon J, Long EA. The heat capacities of uranium, uranium trioxide, and uranium dioxide from 15 K to 300 K. Journal of Chemical Physics. 1952;**20**:695-699. DOI: 10.1063/1.1700518

[145] Tasker IR, O'Hare PAG, Lewis BM, Johnson GK, Cordfunke EHP. Thermochemistry of uranium compounds. XVI. Calorimetric determination of the standard molar enthalpy of formation at 298.15 K, low-temperature heat capacity, and high-temperature enthalpy increments of $UO_2(OH)_2{\cdot}H_2O$ (Schoepite). Canadian Journal of Chemistry. 1988;**66**:620-625. DOI: 10.1139/v88-106

[146] Kubatko KA, Unruh D, Burns PC. Affects of hydrogen peroxide on the stability of Becquerelite. MRS Symposium Proceedings. 2006;**893**:423-428. DOI: 10.1557/PROC-0893-JJ05-19

[147] Shoesmith DW. Used Fuel and Uranium Dioxide Dissolution Studies—A Review; NWMO Technical Report 2007-03. Ontario, Canada: University of Western Ontario; 2014. Available from: https://www.researchgate.net/publication/238622817_Used_Fuel_and_Uranium_Dioxide_Dissolution_Studies_-_A_Review [Accessed: 2018-04-30]

[148] Cox JD, Wagman DD, Medvedev VA. CODATA Key Values for Thermodynamics. New York: Hemisphere Publishing Corp; 1989. ISBN: 0891167587

[149] Gorman-Lewis D, Fein JB, Burns PC, Szymanowski JES, Converse J. Solubility measurements of the uranyl oxide hydrate phases Metaschoepite, Compreignacite, Na–Compreignacite, Becquerelite, and Clarkeite. Journal of Chemical Thermodynamics. 2008;**40**:980-990. DOI: 10.1016/j.jct.2008.02.006

[150] Giammar DE, Hering JG. Influence of dissolved sodium and cesium on uranyl oxide hydrate solubility. Environmental Science and Technology. 2004;**38**:171-179. DOI: 10.1021/es0345672

[151] Sandino A, Bruno J. The solubility of $(UO_2)_3(PO_4)_2{\cdot}4H_2O$(s) and the formation of U(VI) phosphate complexes: Their influence in uranium speciation in natural waters. Geochimica et Cosmochimica Acta. 1992;**56**:4135-4145. DOI: 10.1016/0016-7037(92)90256-I

[152] Bruno J, Sandino A. The solubility of amorphous and crystalline schoepite in neutral to alkaline aqueous solutions. MRS Symposium Proceedings. 1989;**127**:871-878. DOI: 10.1557/PROC-127-871

[153] Meinrath G, Kato Y, Kimura T, Yoshida Z. Solid-aqueous phase equilibria of uranium (VI) under ambient conditions. Radiochimica Acta. 1996;**75**:159-167. DOI: 10.1524/ract.1996.75.3.159

[154] Meinrath G, Kimura T. Behaviour of U(V1) solids under conditions of natural aquatic systems. Inorganic Chimica Acta. 1993;**204**:79-85. DOI: 10.1016/S0020-1693(00)88116-5

[155] Kramer-Schnabel U, Bischoff H, Xi RH, Marx G. Solubility products and complex formation equilibria in the systems uranyl hydroxide and uranyl carbonate at 25°C and I = 0.1 M. Radiochimica Acta. 1992;**56**:183-188. DOI: 10.1524/ract.1992.56.4.183

[156] Rai BD, Felmy AR, Hess NJ, LeGore VL, McCready DE. Thermodynamics of the U(VI)-Ca^{2+}-Cl–OH–H_2O system: Solubility product of becquerelite. Radiochimica Acta. 2002; **90**:495-503. DOI: 10.1524/ract.2002.90.9-11_2002.495

[157] Vochten R, Van Haverbeke L. Transformation of schoepite into the uranyl oxide hydrates: Becquerelite, billietite and wölsendorfite. Mineralogy and Petrology. 1990;**43**: 65-72. DOI: 10.1007/BF01164222

[158] Casas I, Bruno J, Cera E, Finch RJ, Ewing RC. Characterization and dissolution behavior of a becquerelite from Shinkolobwe. Zaire. Geochimica et Cosmochimica Acta. 1997;**61**: 3879-3884. DOI: 10.1016/S0016-7037(97)00195-6

[159] Sandino MCA, Grambow B. Solubility Equilibria in the U(VI)-Ca-K-Cl-H_2O system: Transformation of Schoepite into Becquerelite and Compreignacite. Radiochimica Acta. 1994;**66–67**:37-43. DOI: 10.1524/ract.1994.6667.special-issue.37